

HSM2023-00004

RELATIONSHIP BETWEEN FATIGUE PROPERTIES AND CUTTING PERFORMANCES OF BILAYER TiSiN/TiAlN TOOL COATING

T. Wang^{1,2}, X. Qi³, Y. Wang³, W. Ma³, L. Yan^{4*}, S. Zhang^{1,2*}

¹ Shandong University, Key Laboratory for High Efficiency and Clean Mechanical Manufacture of Ministry of Education, School of Mechanical Engineering, Jinan, China

² Shandong University, Key National Demonstration Center for Experimental Mechanical Engineering Education, Jinan, China

³ Weichai Power Co., Ltd., Weifang, China

⁴ National Huaqiao University, Institute of Manufacturing Engineering, Xiamen, China

*Corresponding author; e-mail: yanlan@hqu.edu.cn; zhangsong@sdu.edu.cn

Abstract

Impact test is a universal method to characterize the fatigue property of coated tools. For the bilayer TiSiN/TiAlN coated tool, the stress state in the cutting process with different feed rates were explored through cutting experiments. A high-temperature and high-frequency impact test platform was built. Through the impact tests with the introduction of the 'pre-loading depth', the fatigue properties and failure mechanisms of coatings under various test conditions were analyzed. Based on the comparative analysis of the results obtained in cutting experiments and impact tests, the mapping relationship between fatigue properties and cutting performances of the coatings was established, thus providing theory and practice foundation for characterization the cutting performance of coated tools under different cutting parameters by high-temperature and high-frequency impact tests.

Keywords:

Coated tool, Impact test, High-frequency, High-temperature, Fatigue property

1 INTRODUCTION

Coated cutting tools have been widely used with the higher requirements of part precision, machining efficiency and surface integrity in the industry. At present, tool coatings have achieved excellent performances in static mechanical properties such as heat resistance, hardness and anti-adhesion [1-3]. However, cutting is a highly dynamic process, where the stress state of tool coating is very complex [4]. The generation of serrated chips will make the coating surface subject to high-frequency cyclic fatigue impact above 1 kHz in the process of turning difficult-to-machine materials, resulting in coating failure. The cyclic mechanical load and thermal load are coupled in a small zone of cutting edge. The response of the coating to this cyclic thermal-mechanical coupling determines its cutting performances [5]. In the performance evaluation of coated tools, the fatigue resistance to cyclic thermal-mechanical coupling load has become a very important index.

In accordance with existing experiments and studies, the impact test is a feasible, efficient and low-cost method to perform cyclic mechanical load on the tool coatings [6,7]. The impact test can effectively simulate the cyclic fatigue impact of coated tools at various frequencies according to

the different cutting processes. It is further close to the actual cutting condition when the heating system is added to the impact test. Beake et al. [8] developed a micro-impact test system with a dual-loading indenter by using an electromagnet and indenter adapter arm, and added a high-temperature system. The controllable impact temperature can reach 600 °C. Lamri et al. [9,10] used the electromagnet to make the rigid indenter obtain constant acceleration and impact the sample material repeatedly in the vertical direction. The impact test machine device integrates a high-efficiency heater, which can increase the test temperature to more than 400 °C. Many experts have developed impact test devices based on different principles. However, the maximum impact frequency of most impact test devices is below 1 kHz. Only a few impact test devices can achieve the impact frequency of more than 1 kHz, but high temperature is not considered in the test.

The high-temperature and high-frequency cycle impact test device based on ultrasonic vibration was developed in this study. The device performed the high-frequency impact on coating samples through a high-frequency reciprocating motion of an ultrasonic horn, whose impact frequency can reach 20 kHz. In addition, a high-temperature module was

added to perform high-frequency fatigue test at high temperature. High-speed titanium alloy cutting experiment and high-temperature impact test were carried out for the bilayer TiSiN/TiAlN coating. The results of the cutting experiment and impact test were compared and analyzed. The mapping relationship between the high-temperature impact test and the cutting experiment was proposed, to characterize and evaluate the cutting performances of coated cutting tools by using the high-temperature impact tests.

2 CUTTING EXPERIMENT

2.1 Experiment setting

Before the impact test, the cutting experiment of the coated tool is required to obtain the basis for setting the impact test parameters. The machine tool used in the cutting experiment is EcoTurn 310 series CNC lathe. This CNC machine tool has high rigidity, high seismic performance, and high dynamic performance spindle drive. The tools are the bilayer TiSiN/TiAlN coating tools. The workpiece material is Ti-6Al-4V titanium alloy. Fig. 1 shows the structure of the bilayer TiSiN/TiAlN coating tool. The parameter settings of cutting experiment are shown in Table 1.

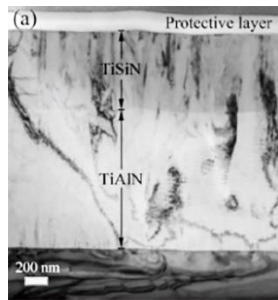


Fig. 1: Structure of the bilayer TiSiN/TiAlN coating tool.

Tab. 1: Parameter settings of cutting experiment.

Cutting amount	Parameter data
Cutting speed (m/min)	40
Feed rate (mm/rev)	0.05; 0.15; 0.25; 0.35
Cutting length (m)	30
Cutting dept (mm)	1

2.2 Chip morphology and geometric parameters

Collect the chips generated in the cutting experiment, polish them, and etch the chips to remove oxides and other impurities on the cross-section of the chips using Kroll reagent (HF: HNO₃: H₂O=2:4:94). The treated chips were observed by scanning electron microscope. The geometric parameters such as the average serration spacing d , the

average serration top height h_{max} , and the average serration root height h_{min} of serration chips are measured. Fig. 2 shows the chip morphology generated in the process of cutting titanium alloy at different feed rates. It can be seen that the chips produced in cutting titanium alloy have obvious serration characteristics [11,12].

The serrated chips will generate high-frequency cyclic alternating fatigue impact on the tool surface, the frequency of this cyclic fatigue impact is consistent with the frequency of serration generation of chips [13,14]. Therefore, the frequency of serration generation can be calculated by the chip geometry parameters, and thus obtain the frequency of the impact acting on the surface of the tool coating. The frequency of serration generation refers to the number of serration agglomerates in the serrated chips generated per unit of time, which is closely related to the frequency of the impact load acting on the surface of the tool. The calculation formula is Formula (1). In the formula, F is the frequency of serration generation; V_c is the cutting speed. Table 2 shows the serrated chip geometry parameters and serration generation frequency at different feed rates. Measurement and calculation results indicate that the frequency of chip serration generation is approximately 3-23 kHz under the condition of feed rate of 0.05-0.35 mm/rev. It can be inferred that the tool coating will be subjected to high-frequency cyclic fatigue impacts, and these high-frequency impacts are an important factor causing coating wear.

$$F = \frac{V_c}{d} \quad (1)$$

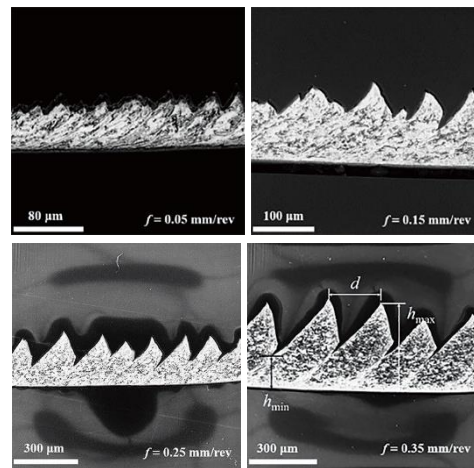


Fig. 2: Chip morphologies at different feed rates.

2.3 Cutting temperature

Temperature of the tool-chip contact center in the cutting process is obtained through the AdvantEdge FEM. The temperature of the tool-chip contact center is about 500-700 °C, as shown in Fig.3, which indicates that a series of tool wear occurs in this temperature range during the cutting process.

Tab. 2: Serrated chip geometry parameters and serration generation frequency.

Feed rate f (mm/rev)	Average serration spacing d (mm)	Average serration top height h_{max} (mm)	Average serration root height h_{min} (mm)	Frequency of serration generation F (kHz)
0.05	0.029±0.027	0.057±0.015	0.041±0.007	22.982±1.255
0.15	0.087±0.006	0.125±0.015	0.072±0.007	7.660±1.312
0.25	0.146±0.014	0.199±0.047	0.074±0.013	4.572±0.248
0.35	0.241±0.042	0.332±0.009	0.118±0.021	2.775±0.471

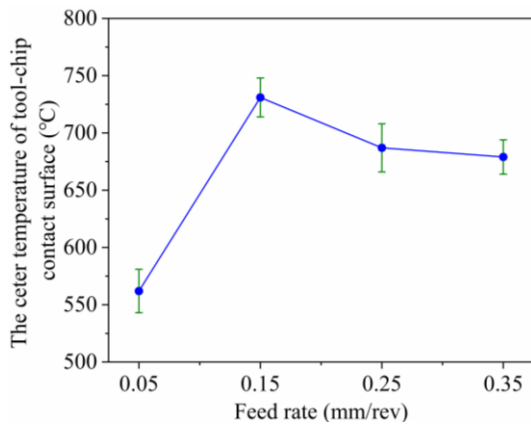


Fig. 3: Temperature of the tool-chip contact center.

3 IMPACT TEST

3.1 Impact test Device

The diagram of the high-frequency cyclic impact test device is shown in Fig. 4. The impact frequency of the impact test can reach 20 kHz through the ultrasonic actuator control unit. The test device is mainly composed of the motion module, ultrasonic high-frequency vibration system module and data acquisition module. The specimen and the Rockwell diamond indenter are fixed on the XY table and the linear driving system. The amplitude mode and duration of the sample are controlled by the ultrasonic driver. A force sensor with a sampling frequency of 27 kHz is used to measure the dynamic load signal during the cyclic impact test. The sampling frequency of 27 kHz ensures that the maximum amplitude of each waveform is captured during the impact process. The cutting process is a thermo-mechanical coupling process. Based on the high-frequency impact test device, a high-temperature furnace and a high-temperature control system are installed to carry out high-frequency impact test in a simulated environment close to the actual cutting temperature. The high-temperature system can make the test temperature of impact test reach 800 °C. The schematic diagram of the high-temperature furnace is shown in Fig. 5. During the high-temperature impact test, the high-frequency impact process of the indenter and the sample is carried out in the furnace chamber. Since the materials of the force sensor and the ultrasonic horn cannot withstand the high temperature of more than 400 °C, an extension rod fixture made of high temperature resistant nickel base alloy GH3128 is designed to achieve the normal operation in high temperature. The fixture is fixed on both ends of the force sensor and the ultrasonic horn through the thread to ensure the normal contact between the indenter and the sample in the high-temperature furnace cavity. The site layout of the high-temperature and high-frequency impact test is shown in Fig. 6.

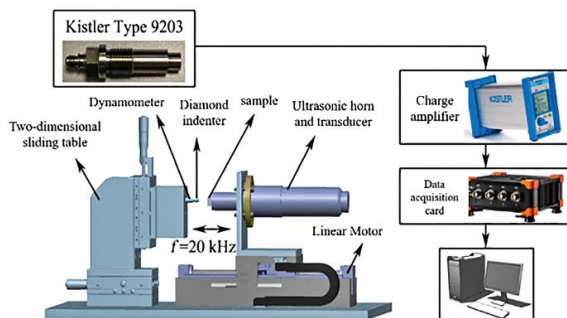


Fig. 4: Device diagram.

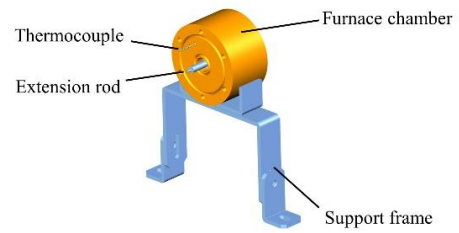


Fig. 5: High-temperature furnace.

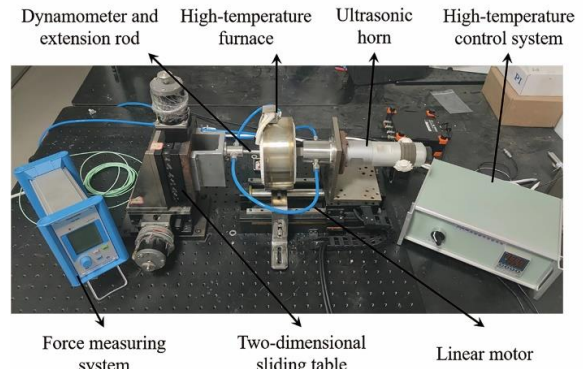


Fig. 6: Site layout of impact test.

3.2 Test principle

Previous studies have shown that in addition to the alternating cyclic stress, the tool coating will receive continuous minimum stress during the cutting process, which is called 'pre-stress' [15]. The existing impact test does not consider the phenomenon of pre-stress. In this study, 'pre-loading depth' was set in the high-temperature and high-frequency impact test, the indenter was pressed into the coating sample to a certain depth before the cycle of high-frequency impact, to simulate the pre-stress phenomenon of the tool coating in actual cutting.

During the impact test, primarily, ensure that the coating sample is in critical contact with the indenter. The coating sample is adhered to the end of the ultrasonic horn and installed on the linear motor together. Through the horizontal movement of the linear motor, the coating sample slowly approaches the indenter until it contacts. When the contact force signal between the coating sample and the indenter reaches 0.01 N, it is considered that the critical contact condition is reached. Subsequently, start the high-temperature furnace. When the temperature in the furnace rises to the required temperature, the indenter is driven to press into the coating sample by a certain depth (pre-loading depth) through the linear motor, then turned on the power supply of the ultrasonic generator. The coating sample moves in a high-frequency cycle with the ultrasonic horn, and the indenter will produce a high-frequency cyclic impact on the coating sample. The number of impact cycles is controlled by setting the impact time. Fig. 7 shows the schematic diagram of the procedure of the impact test.

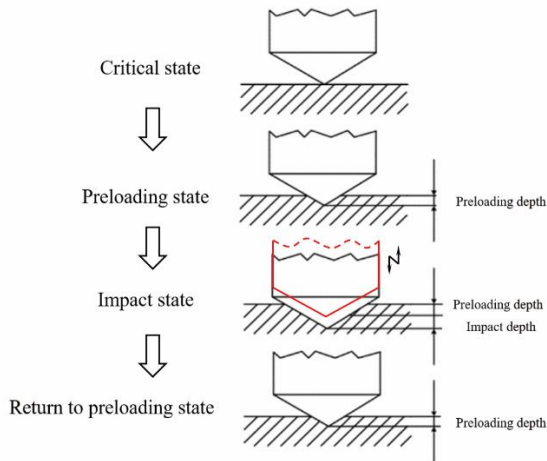


Fig. 7: Schematic diagram of the impact test.

3.3 Design of impact test

The samples of high-temperature and high-frequency impact test are $8 \times 8 \times 3$ mm sample pieces made of bilayer TiSiN/TiAlN coatings. The indenter is a Rockwell conical diamond indenter with a fillet radius of 0.05 mm. One end of the dynamometer is installed with an indenter, and the other end is connected to a charge amplifier. The coating sample piece is fixed on the vibration output end of the ultrasonic horn, and the ultrasonic horn is fixed on the linear motor through threads so that it can move in the horizontal direction. In the high-temperature and high-frequency impact test, the impact time is set to 2 s, scilicet, the number of impacts is 40,000 times, and the impact depth H (half of the amplitude) is set to $3 \mu\text{m}$. The pre-loading depth h_p can be calculated from the average serration root height h_{\min} and the average serration top height h_{\max} in the serrated chip geometry parameters detected in the cutting experiment. The calculation formula is shown in Formula (2). The impact temperature is set based on the tool-chip contact center temperature obtained in the finite element simulation. In summary, the parameter settings of the high-temperature and high-frequency impact test are shown in Table 3.

$$\frac{2H + h_p}{h_p} = \frac{h_{\max}}{h_{\min}} \quad (2)$$

Tab. 3: Parameter settings of the high-temperature and high-frequency impact test.

Impact depth H (μm)	Pre-loading depth h_p (μm)	Impact temperature ($^{\circ}\text{C}$)
3	9.00; 7.51; 18.00	400; 500; 600; 700

4 RELATIONSHIP BETWEEN IMPACT PROPERTY AND CUTTING PERFORMANCES

The impact force of the coating in the high-temperature and high-frequency impact test is monitored in real-time. Fig. 8 shows the trend diagram of the impact force with time. Tables 4 and 5 show the pre-loading depth force and fatigue impact force of the coatings at different temperatures and pre-loading depths in the high-temperature and high-frequency impact test.

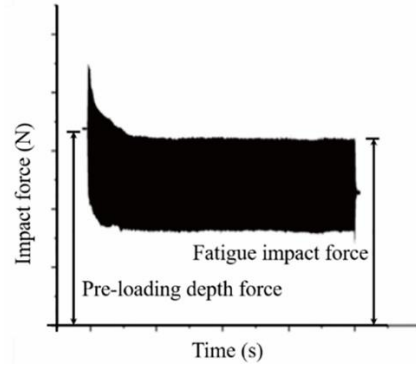


Fig. 8: Trend diagram of the impact force.

Tab. 4: Pre-loading depth force.

	7.51 μm	9.00 μm	18.00 μm
400 $^{\circ}\text{C}$	4.97 N	6.99 N	13.87 N
500 $^{\circ}\text{C}$	5.06 N	5.44 N	12.48 N
600 $^{\circ}\text{C}$	3.21 N	5.13 N	10.64 N
700 $^{\circ}\text{C}$	2.16 N	4.26 N	8.36 N

Tab. 5: Fatigue impact force.

	7.51 μm	9.00 μm	18.00 μm
400 $^{\circ}\text{C}$	5.62 N	8.47N	25.98 N
500 $^{\circ}\text{C}$	7.25 N	6.99 N	14.20 N
600 $^{\circ}\text{C}$	3.11 N	6.64 N	11.61 N
700 $^{\circ}\text{C}$	2.27 N	4.97 N	9.89 N

According to the real-time monitoring of the impact force during the impact, the impact stress on the surface of the coating can be calculated, to construct the alternating stress map of the surface of the coating during the impact test. In the high-frequency impact test, the impact frequency set by the ultrasonic generator is 20 kHz, which means that the alternating frequency of the stress on the coating during the impact is also 20 kHz. The ratio of the impact force value N in the fatigue stage on the tool coating to the actual contact area S between the indenter and the coating surface is equal to the maximum contact stress σ'_{\max} experienced by the coating surface, as shown in Formula (3). The pre-stress σ_p received by the coating during the impact can be calculated from the ratio of the pre-loading depth force N_p to the actual contact area S between the indenter and the coating surface, as shown in Formula (4). So far, the data needed to construct the alternating stress map of the coating in the high-temperature and high-frequency impact test can be obtained.

$$\sigma'_{\max} = \frac{N}{S} \quad (3)$$

$$\sigma_p = \frac{N_p}{S} \quad (4)$$

The alternating stress map of the tool coating in the cutting experiment can also be obtained by similar way. The dynamometer collects the main cutting force in the cutting process, and the average cutting force N_{avg} can be obtained after processing. Fig. 9 shows the formation model of the serrated chip. The chip load can be idealized as a periodic alternating cycle state. Its peak and trough represent the

maximum cutting force N_{max} (or the maximum contact stress) and the minimum cutting force N_{min} (or the minimum contact stress) acting on the coated tool respectively. The intermediate equilibrium position represents the average cutting force N_{avg} (or the average contact stress) acting on the coated tool. Combined with the geometric parameters of the serrated chip, it can be considered that the ratio of the maximum cutting force N_{max} to the minimum cutting force N_{min} (i.e. the ratio of the maximum contact stress to the minimum contact stress) is equal to the ratio of the average serration height h_{max} to the average root height h_{min} . The average contact stress σ_{avg} can be calculated according to the ratio of the average normal force N_{avg} acting on the coated tool to the wear area S_w of the coated tool, as shown in Formula (5). The maximum contact stress σ'_{max} and the minimum contact stress σ'_p can be calculated according to Formula (6). Thus the alternating amplitude of contact stress A can also be obtained.

$$\sigma_{avg} = \frac{N_{avg}}{S_w} \quad (5)$$

$$\frac{\sigma_{max}}{\sigma_{min}} = \frac{h_{max}}{h_{min}} \quad (6)$$

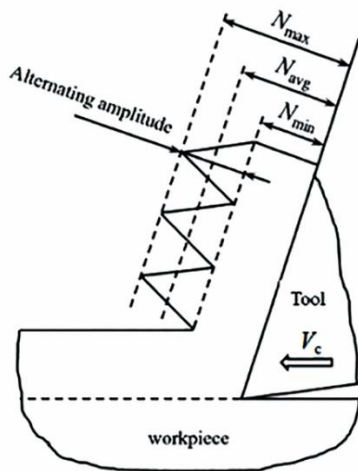
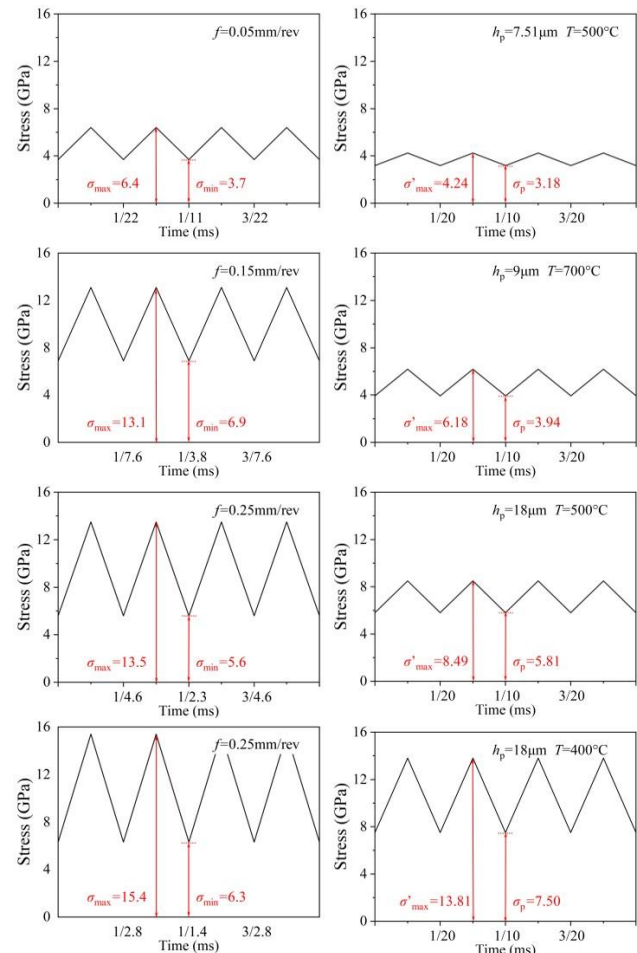


Fig. 9: Serrated chip formation model in Ti-6Al-4V turning with coated tools.

Based on the above calculation, the alternating stress map of the coating in the impact test and cutting experiment can be obtained. To further more intuitively show the simulation of the stress state of the coating in the actual cutting experiment by the high-temperature and high-frequency impact test, the cutting alternating stress map under different feed rates and the corresponding impact alternating stress map under different temperatures and preloading depths are compared, as shown in Fig.10. In the actual cutting process, the tool is not only subjected to the stress impact of serrated chips, but also to impacts caused by factors such as vibration and noise. From the stress map, it can be seen that the alternating stress on the cutting tool in the cutting experiment is higher than that in the impact test. Therefore, the magnitude and trend of stress are the key points for comparing the two stress maps.

After comparing the alternating stress maps, the stress of both is on an order of magnitude, and the stress value in the impact test is generally smaller. In the future, it is worth studying how to accurately control the value of the alternating stress in the impact test to make it closer to the cutting experiment. From the change trend of the

alternating stress, there is a certain connection: the maximum stress increases gradually with the increase of feed rate (or pre-press depth), and the alternating amplitude also increases gradually. And the alternating serration is more and more obvious from the shape point of view. This phenomenon is also consistent with the morphology change of serrated chips. In general, the impact test can effectively simulate the real stress state of the tool coating in the cutting process, and the alternating stress state of the tool coating in the two tests is very close. From this, it can be inferred that in the cutting experiments and impact tests under the similar alternating stress state, the wear morphology and failure mechanism should also be related to a certain extent.



(a) Cutting experiment (b) Impact test

Fig. 10: Comparison of alternating stress maps.

5 CONCLUSION

In this paper, the bilayer TiSiN/TiAlN tool coating is taken as the research object to carry out cutting experiments and high-temperature and high-frequency impact tests. The cutting performances and fatigue properties of bilayer TiSiN/TiAlN tool coating are explored. The mapping relationship between fatigue properties and cutting performances of the coating is established by combination with the alternating stress of the coating. The main conclusions can be summarized as follows:

- (1) A high-temperature and high-frequency impact test platform is built to study the fatigue property and fatigue failure mechanism of coating, the impact frequency in tests can reach 20kHz.

(2) Pre-loading depth is introduced to simulate the actual stress state of the coating tool during cutting, which makes the high-frequency impact test more reliable and practical.

(3) The change trend of alternating stress of coating in cutting experiments and impact tests is consistent.

(4) High-temperature and high-frequency impact test can obtain the coating fatigue properties under different working conditions, thus characterizing its cutting performances under different cutting parameters.

6 ACKNOWLEDGMENTS

This work was supported by Taishan Scholar Project of Shandong Province (No. ts201712002). This work has received assistance from Institute of Manufacturing Engineering of National Huaqiao University in experiments and tests.

7 REFERENCES

- [Blinkov 2018] Blinkov I V., et al. Heat Resistance, High-Temperature Tribological Characteristics, and Electrochemical Behavior of Arc-PVD Nanostructural Multilayer Ti-Al-Si-N Coatings. *Protection of Metals and Physical Chemistry of Surfaces*, 2018, Vol.54, No.3., pp 269-279.
- [Antonyuk 2008] Antonyuk V S., et al. Providing adhesion strength for a substrate-coating system under contact loading. *Journal of Superhard Materials*, 2008, Vol.30, No.2., pp 133.
- [Wang 2019] Wang H., et al. Corrosion resistance enhancement of WC cermet coating by carbides alloying. *Corrosion Science*, 2019, Vol.147., pp 372-383.
- [Li 2022] Li G., et al. Machinability of additively manufactured titanium alloys: A comprehensive review. *Journal of manufacturing processes*, 2022, Vol.75., pp 72-99.
- [Pramanik 2014] Pramanik A. Problems and solutions in machining of titanium alloys. *International Journal of Advanced Manufacturing Technology*, 2014, Vol.70., pp 919-928.
- [Zha 2021] Zha X., et al. Correlation of the fatigue impact resistance of bilayer and nanolayered PVD coatings with their cutting performance in machining Ti-6Al-4V. *Ceramics International*, 2021, Vol.45., pp 14704-14717.
- [Wang 2021] Wang T., et al. Mechanical impact test methods for hard coatings of cutting tools: a review. *The International Journal of Advanced Manufacturing Technology*, 2021, Vol.115, No.5., pp 1367-1385.
- [Beake 2019] Beake B D., et al. Elevated temperature micro-impact testing of TiAlSiN coatings produced by physical vapour deposition. *Thin Solid Films*, 2019, Vol.668., pp 137358.1-137358.9.
- [Lamri 2013] Lamri S., et al. Damage phenomena of thin hard coatings submitted to repeated impacts: Influence of the substrate and film properties. *Materials Science & Engineering A Structural Materials Properties Microstructure & Processing*, 2013, Vol.560., pp 296-305.
- [Lamri 2010] Lamri S., et al. Failure Mechanisms of Thin Hard Coatings Submitted to Repeated Impacts: Influence of the Film Thickness. *Advanced Materials Research*, 2010, Vol.112., pp 73-82.
- [Su 2015] Su G., et al. Influences of chip serration on micro-topography of machined surface in high-speed cutting. *International Journal of Machine Tools & Manufacture*, 2015, Vol.89., pp 202-207.
- [Upadhyay 2012] Upadhyay V., et al. Modelling and experimental study of chip serration frequency in dry turning of Ti-6Al-4V alloy. *International Journal of Machining and Machinability of Materials*, 2012, Vol.12, No.4., pp 358-371.
- [Arriola 2011] Arriola I., et al. Relationship between machinability index and in-process parameters during orthogonal cutting of steels. *CIRP Annals - Manufacturing Technology*, 2011, Vol.60, No.1., pp 93-96.
- [Baizeau 2016] Baizeau T., et al. Cutting force sensor based on digital image correlation for segmented chip formation analysis. *Journal of Materials Processing Technology*, 2016, Vol.238., pp 466-473.
- [Wang 2021] Wang T., et al. Research on cutting performance of coated cutting tools by a new impact test method considering contact stress condition caused by segmented chips. *Journal of Manufacturing Processes*, 2021, Vol.68., pp 1569-1584.